Antarctic Science 27(4), 403–410 (2015) © Antarctic Science Ltd 2015 doi:10.1017/S0954102014000832

Spatial–temporal patterns of surface melting observed over Antarctic ice shelves using scatterometer data

SANDIP RASHMIKANT OZA

Space Applications Centre (ISRO), Ahmedabad 380 015, India
sandip.r.oza@gmail.com

Abstract: Ice shelves fringing Antarctica are sensitive indicators of climate change due to the direct interface with the atmosphere and ocean. Meltwater induced by atmospheric warming percolates from the surface into hydrofractures and affects shelf stability. Surface melting reduces the microwave backscattering; thus backscatter data is useful in melt monitoring. The Ku-band scatterometer derived melting index (MI) was utilized to assess the decadal (2000–10) variability observed over Antarctic ice shelves. The low intensity melting observed over large ice shelves and high intensity melting observed over the Larsen, Amery, West and Shackleton ice shelves are discussed. A correlation of around 93% was observed between MI variation and rift propagation over Amery Ice Shelf. The El Niño and the Southern Oscillation (ENSO) correlation with MI was also investigated. The paper highlights that scatterometer derived information has the potential to assess meltwater production and rift propagation.

Received 24 January 2014, accepted 10 September 2014, first published online 18 February 2015

Key words: Amery Ice Shelf, melting index, OSCAT, QuikSCAT, rift propagation

Introduction

Dynamic response of ice sheets to warming is the largest unknown in the projection of sea level change (Allison *et al.* 2009). The average rate of ice loss from the Antarctic ice sheet has probably increased from 30 Gt yr^{-1} over the period 1992–2001 to 147 Gt yr^{-1} over the period 2002–11 (IPCC 2013). The Antarctic ice sheet loses mass at its ice shelves bordering the Southern Ocean (Hellmer *et al.* 2012). These ice shelves are sensitive indicators of climate change due to their direct contact with both atmosphere and ocean.

It is probable that ice shelves will undergo enhanced melting (surface and basal) and increased calving in a warming climate (IPCC 2013). Munneke *et al.* (2014) suggested that significant mass loss from these ice shelves is due to the process of hydrofracturing, whereby a water-filled crevasse is opened by the hydrostatic pressure acting at the crevasse tip. Meltwater drips down into cracks; when it refreezes the cracks expand, weakening the shelf stability (Scambos *et al.* 2008).

Scatterometer derived melt information have been reported and discussed in detailed by Liu *et al.* (2006), Trusel *et al.* (2012) and Wismann (2000). Oza *et al.* (2011) evaluated the surface melting observed over Amery Ice Shelf (AIS) using QuikSCAT scatterometer data using the 'temporal reduction in backscatter (TRB)' technique.

The spatial and temporal distribution of the melting index (MI) observed over Antarctic ice shelves, with special emphasis on Larsen C Ice Shelf (LIS) in West Antarctica, and AIS, West (WIS) and Shackleton (SIS) ice shelves in East Antarctica are described here. The association of interannual variations of MI with AIS rift propagation are also investigated. Further, the tropical linkage of MI is discussed.

Data

Scatterometer data

Daily composite QuikSCAT backscatter data of HH polarization (σ_H) at 4.45 km resolution (Early & Long 2001) were used for the study. Mid-month data from January 2000 to July 2009 were obtained from the NASA sponsored Scatterometer Climate Record Pathfinder at Brigham Young University (http://scp.byu.edu). The backscatter time series data from QuikSCAT was extended by data available from Oceansat-2 OSCAT scatterometer for 2009–10. The enhanced resolution OSCAT data (at 25 km) was generated using the 'drop in bucket' method (Long & Drinkwater 1994) from the L2A swath data. Mid-November data was utilized to normalize OSCAT data with respect to QuikSCAT data. Bhowmick *et al.* (2014) reported that the difference between the average backscattering coefficients of these two sensors over Antarctica is lower than 0.25 dB.

RADARSAT data

RADARSAT-2 ScanSAR Wide Sigma-0 data (50 m resolution) was acquired on 10 February 2013 for the assessment of ice deformation taking place over AIS. Advancement in AIS rift length was assessed by comparing 2013 data with the Sigma-0 (25 m resolution)

https://doi.org/10.1017/S0954102014000832 Published online by Cambridge University Press

data for 2000, obtained from the RADARSAT-1 Antarctic Mapping Project (RAMP; http://bprc.osu.edu/rsl/radarsat/data/). Both datasets were co-registered using pseudo invariant ice features. The error in the identification could be of the order of 50 m.

Moderate resolution imaging spectroradiometer data

Data for each December–January–February period for 2002–10 (Scambos *et al.* 1996) from the moderate resolution imaging spectroradiometer (MODIS; 250 m resolution) were obtained from the National Snow and Ice Data Center (NSIDC). Similar to Walker *et al.* (2013), we performed contrast stretching, toning and brightening of the images to enhance the visibility of rifts.

Ancillary data

Time series of cumulative melting surface index derived by Picard & Fily (2006) was obtained for AIS (http://lgge.osug.fr/~picard/melting/) and utilized to validate scatterometer derived MI. The automatic weather station (AWS) data was obtained from the Australian Antarctic Division (http://data.aad.gov.au/aadc) for the Davis station (68°35'S, 77°58'E) near to AIS. The AWS data was utilized to compute the sum of December and January monthly average air temperature for each summer.

Methodology

Computation of melting index

Snow is an inhomogeneous medium consisting of ice particles, air and liquid water (if wet). The backscattering coefficient of snow is highly dependent on the wetness and roughness of the snow cover (Fung 1994). In case of wet snow, surface scattering dominates over volume scattering. The presence of liquid water in snow volume also causes an increase in the dielectric loss factor of the layer, which increases the absorption coefficient and reduces the penetration depth. During summer, the penetration depth reduces to the uppermost 3–4 cm (Liu *et al* 2006), resulting in a decrease in backscatter values.

The TRB technique has been utilized by Wismann (2000) for monitoring seasonal snow melt over Greenland using the European Remote Sensing satellite (ERS) scatterometer data. Oza *et al.* (2011) demonstrated the use of the TRB approach for monitoring surface melting over AIS. A similar approach was followed using QuikSCAT and Oceansat-2 OSCAT backscatter data of σ_H to investigate the spatially varying pattern of MI, defined as:

$$\mathrm{MI} = \Sigma\,(\sigma_{\mathrm{wH}}\text{-}\sigma_{\mathrm{si}})(\mathrm{dB});\quad \text{sum from i} = \text{October to i} = \text{January}. \qquad (1)$$

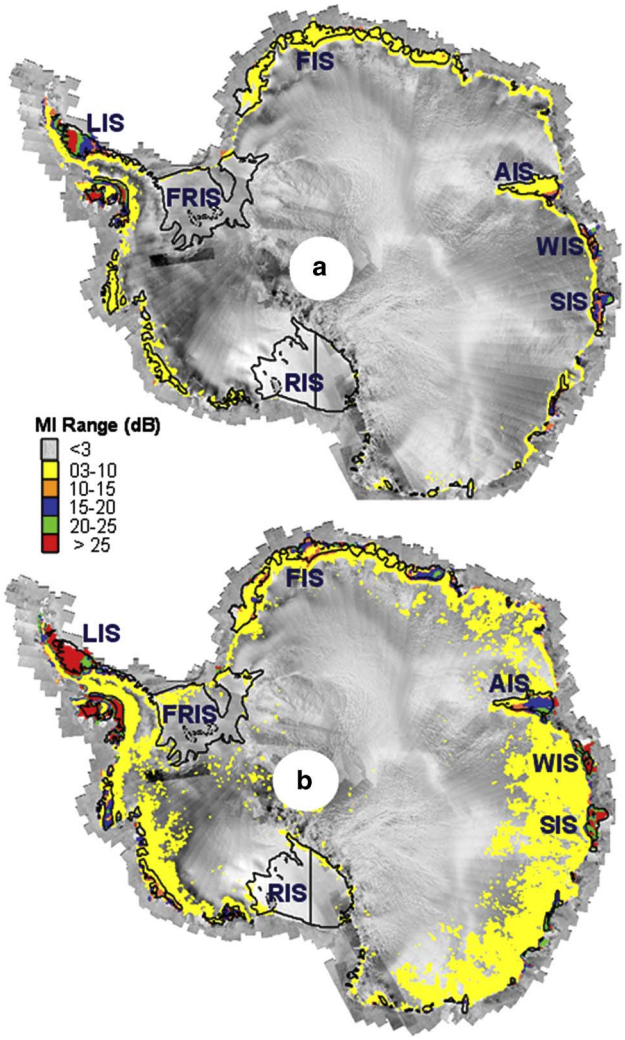


Fig. 1. Decadal (2000–10) **a.** average ($\mathrm{MI_{av}}$) and **b.** maximum ($\mathrm{MI_{mx}}$) statistics of melting index (MI). The MI classes are overlaid on the RADARSAT Antarctic Mosaic obtained from RAMP. AIS = Amery, FIS = Fimbul, FRIS = Filchner-Ronne, LIS = Larsen C, RIS = Ross, SIS = Shackleton, WIS = West ice shelves.

Here, σ_{wH} is the average σ_H for March to September of the preceding winter, and σ_{si} is the mid-month σ_H for each month (denoted 'i') from October to January. Therefore, MI (in dB) is the cumulative TRB for October to January and describes a temporally integrated reduction in σ_H, which can be taken as an indicator of the magnitude of surface melting during the spring and summer.

Assessment of Amery Ice Shelf rift propagation

Interannual variations observed over AIS were analysed to assess the impact of surface melting on the propagation of rifts. The assessment was carried out over the rift system of AIS. This active rift system consists of two longitudinal-to-flow rifts ~30 km apart that initiated

https://doi.org/10.1017/S0954102014000832 Published online by Cambridge University Press

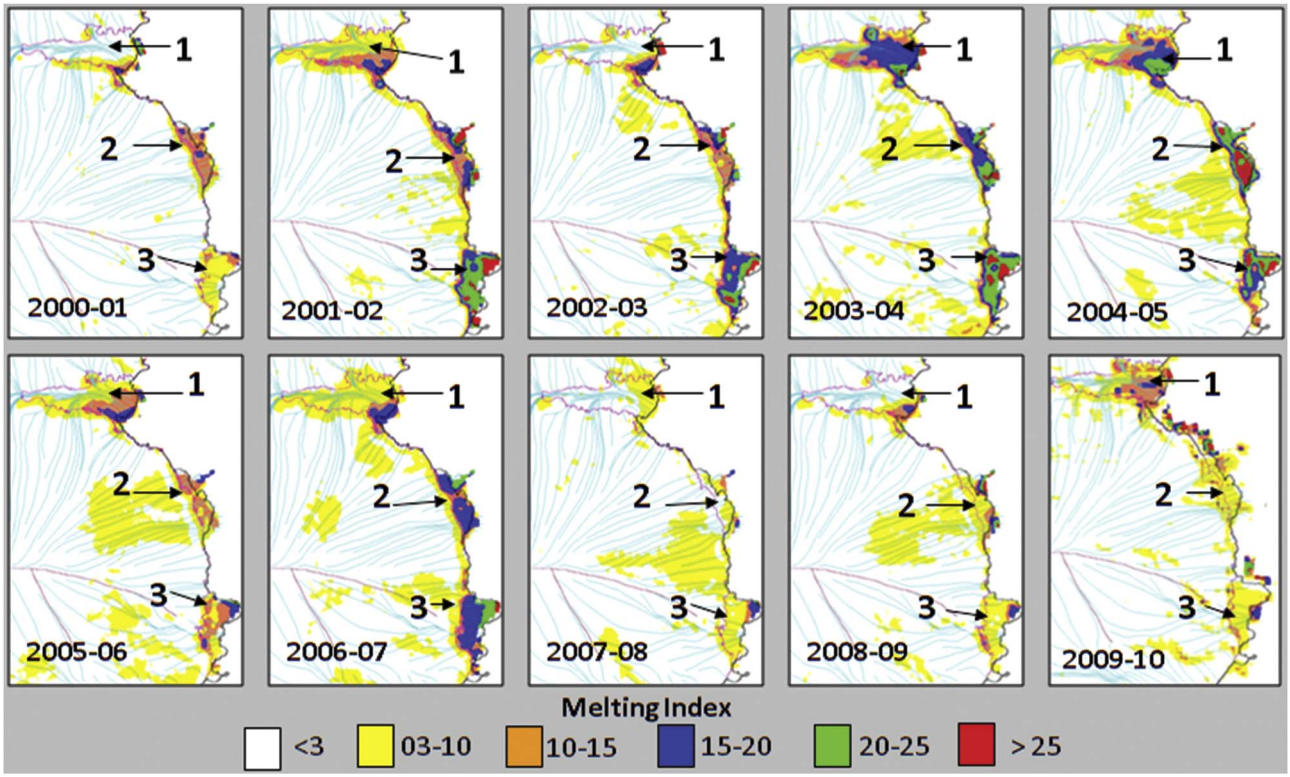


Fig. 2. Spatial distribution of melting index (MI; dB) for the Amery Ice Shelf (1), West Ice Shelf (2) and Shackleton Ice Shelf (3) for each summer from 2000–01 to 2009–10. RAMP ice flow lines are shown in cyan and ice divide lines in maroon. Years 2000–01 to 2008–09 are derived from QuikSCAT scatterometer data, while 2009–10 is derived from OSCAT scatterometer data.

~25 years ago and two transverse-to-flow rifts (Bassis *et al.* 2007). Rift length was measured by following the side wall from triple junction point to the tip on the MODIS imagery. The possible error in the identification could be of the order of one MODIS pixel (250 m). The rate of AIS rift propagation reported by Fricker *et al.* (2005) for the common period of 2001–04 was also utilized to assess the impact of surface melting.

Southern Oscillation Index correlation with melting index

The National Centers for Environmental Prediction (NCEP) and the National Center for Atmospheric Research (NCAR) reanalysis monthly surface air temperature (2.5° x 2.5° gridded data) was utilized to assess the impact of atmospheric warming on MI. The El Niño and Southern Oscillation (ENSO) index correlation with surface melting was also investigated. The ENSO is an ocean–atmosphere oscillation manifested in shifting sea surface temperature anomalies in the tropical Pacific Ocean, and its variability is often measured by the 'see-saw' of surface pressure anomalies between Tahiti and Darwin (Tedesco & Monaghan 2009). This is also known as the Southern Oscillation Index (SOI) and is significantly correlated with surface melting. The SOI data was obtained from the Earth System Research Laboratory Physical Sciences Division (Boulder, CO, http://www.esrl.noaa.gov/psd/).

The following three empirical relationships were investigated to study the impact of air temperature (T_a) and SOI on MI:

$$MI = a_1 \times T_a + a_2 \quad (2)$$

$$MI = b_1 \times SOI + b_2 \quad (3)$$

$$MI = c_1 \times T_a + c_2 \times SOI + c_3, \quad (4)$$

where T_a is the sum of December and January monthly average air temperatures, SOI is averaged October to January and MI is the spatial–temporal average MI value of ice shelves. The regression coefficients are denoted by a, b and c.

Results

Spatial–temporal pattern of melting index

The distribution pattern of MI (Fig. 1) highlights large-scale surface melting events taking place around Antarctica. High values (> 20 dB) for the decade-averaged value, denoted MI_{av} (Fig. 1a), and the decade-maximum

https://doi.org/10.1017/S0954102014000832 Published online by Cambridge University Press

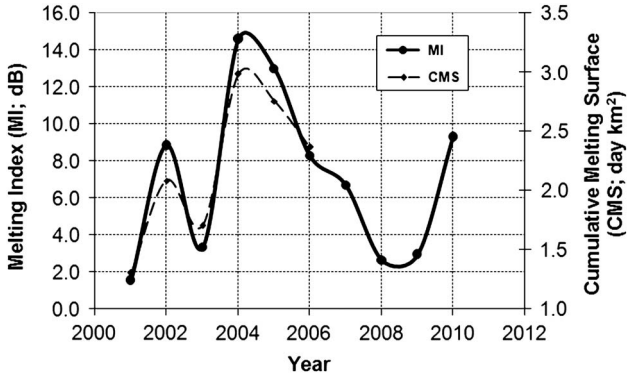


Fig. 3. Interannual variations of surface melting for AIS, determined from melting index (MI; dB) and cumulative melting surface index (CMS; day km^2).

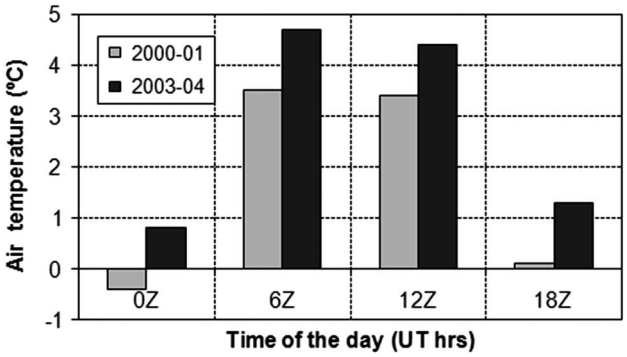


Fig. 4. Sum of December and January monthly average air temperatures recorded at Davis Station.

value, MI_{mx}, (Fig. 1b) were observed over LIS. This is indicative of consistent high intensity summer melting over a decade. Low intensity surface melting (< 3 dB per summer) was evident over the large Filchner-Ronne (FRIS) and Ross (RIS) ice shelves. The average value of the cumulative melting surface index (CMS; day km^2) during 2001–06 over the FRIS region was 0.21 day km^2 versus 8.5 day km^2 for the Peninsula region. The lower CMS value observed over FRIS supports the low intensity melting apparent in this region. As with LIS in West Antarctica, SIS and WIS in East Antarctica also showed high MI_{mx} and MI_{av}. This suggests that East Antarctic ice shelves are not immune to the effect of warming.

Melting index pattern over Amery Ice Shelf

Over the AIS, a significant difference (Fig. 1) was seen between MI_{mx} (10–25 dB) and MI_{av} (< 10 dB). The spatial distributions of MI plotted for each summer show high interannual variability (Fig. 2). The finer pattern visible over ice shelves from 2000–01 to 2008–09 is missing in 2009–10, possibly due to the coarser spatial resolution of OSCAT data. High correlation (r = 0.98) found between MI and CMS variations (Fig. 3) confirms the validity of MI derived from mid-month scatterometer data.

As evident from Fig. 3, MI averaged over AIS was lowest in 2000–01 (< 2 dB) and highest in 2003–04 (> 14 dB). The cumulative December and January monthly average air temperature data (Fig. 4) highlights that the temperatures observed at 00h00 and 18h00 in

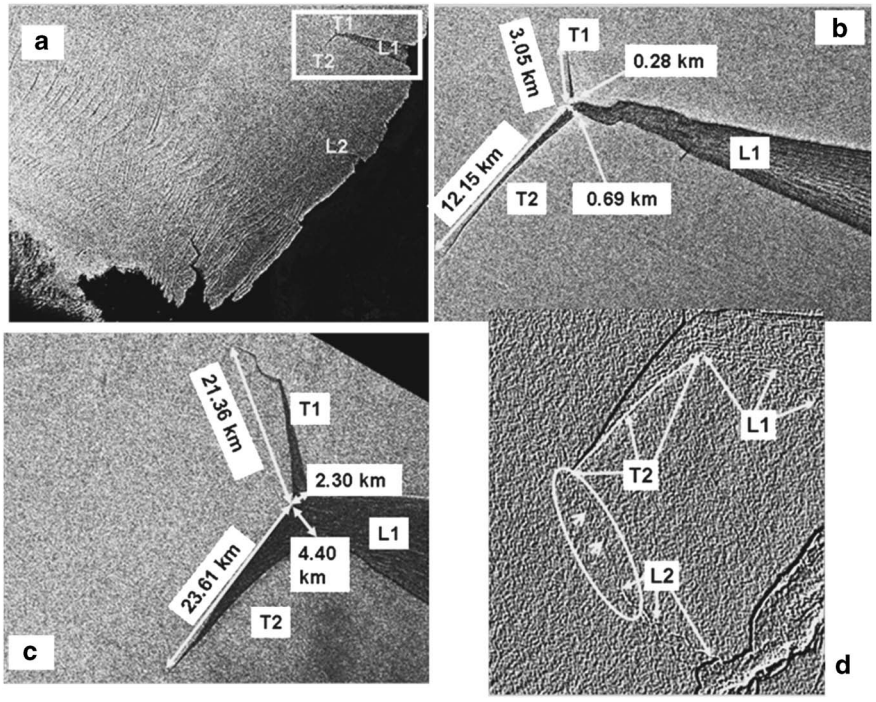


Fig. 5a. Amery Ice Shelf covering the L1-L2-T1-T2 rift system. Status of rift system in **b.** 2000 and **c.** 2013. **d.** Status of the 'loose tooth' in 2013, a linear deformation feature is visible in the encircled region highlighted by arrows.

https://doi.org/10.1017/S0954102014000832 Published online by Cambridge University Press

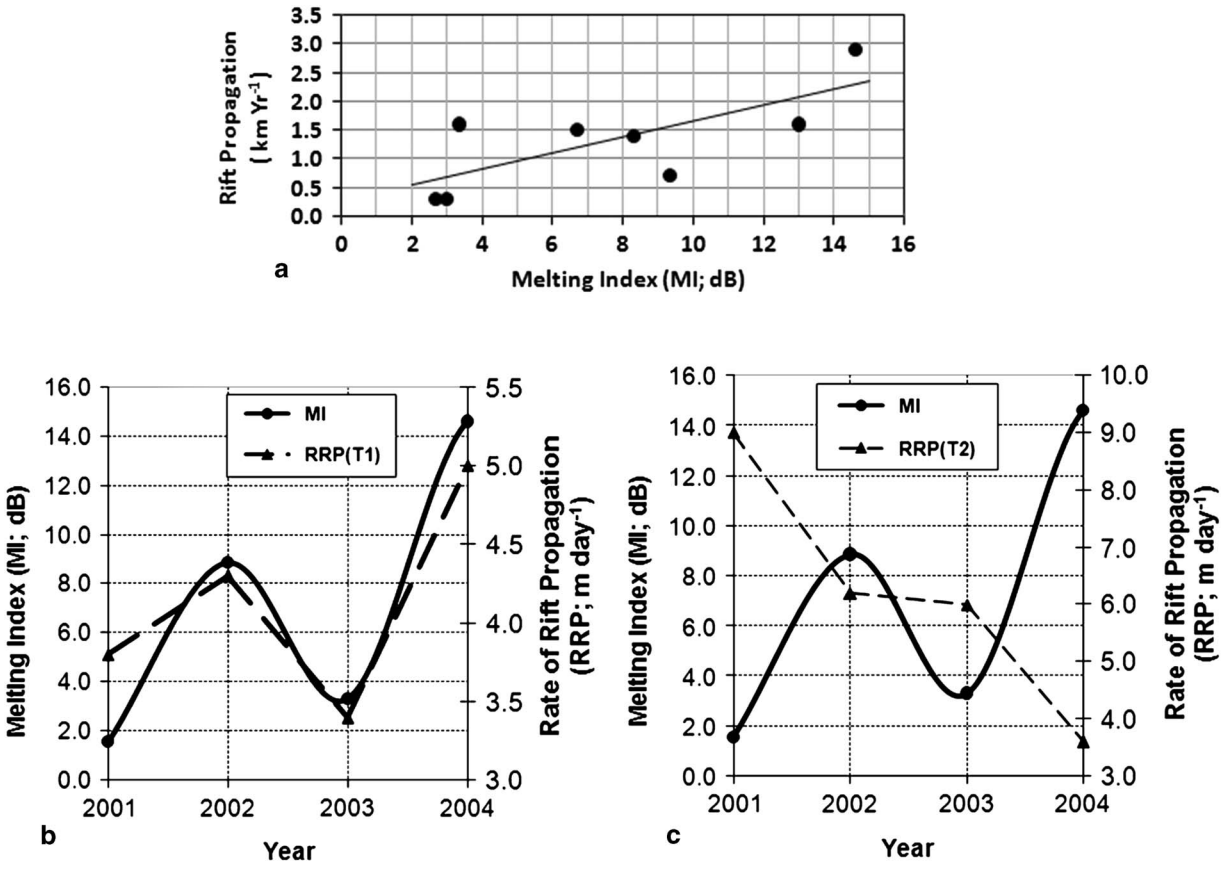


Fig. 6. Interannual variations in melting index (MI; dB) and rate of rift propagation. **a.** Correlation between MI and rift propagation (km yr^{-1}). Rate of rift propagation (m day^{-1}) for **b.** T1 and **c.** T2.

2000–01 were either near-zero or subzero, whereas in 2003–04 it was ~1°C or higher. Moreover, in 2003–04 at 06h00 and 12h00 temperatures were >4°C. The subzero temperatures recorded at 00h00 and 18h00 in 2000–01 could have resulted in refreezing of meltwater produced during the warmer period between 06h00 to 12h00, which is reflected in the lower MI observed in 2000–01.

Present status of Amery Ice Shelf rift system

Over the area of AIS covering a rift system (L1-L2-T1-T2; Fig. 5), MI_{mx} was >15 dB and MI_{av} was >10 dB (Fig. 1).

Examination of the shift in the tip of the L1-T1-T2 junction point indicates an advancement of ~16 km from 2000 to 2013 (Fig. 5). It is apparent that connection between the tips of L2 and T2 will lead to disintegration of a large tabular iceberg from AIS. On the RADARSAT image (Fig. 5d), a deformation feature is visible that originates from the tip of L2 and extends towards the tip of T2. This feature indicates the possibility of detachment of a ~ 800 km^2 tabular iceberg, also known as the 'loose tooth' (Fricker *et al.* 2005).

Between 2000 and 2013, a larger increase in the length of T1 (~ 18 km) was observed compared to T2 (~ 11.5 km) (Fig. 5b & c). However, the increase in width for T2 (~ 3.7 km) was ~ 1.8 times that observed for T1 (~ 2.0 km).

Impact of melting index on Amery Ice Shelf rift propagation

The relationship between MI and rift propagation (P; the increase in length from previous year) for T1 was investigated using a longer time series (2003–10). The following empirical relationship (Fig. 6a) was obtained, which indicates that propagation distance per year increases with the increase in surface melting:

$$P = 0.1616 \times MI;\ r^2 = 0.86;\ SE = 0.60 \qquad (5)$$

Association of the rate of rift propagation (RRP; m day^{-1}) data (Fricker *et al.* 2005) with surface melting is shown in Fig. 6b & c. As observed in Fig. 6b, interannual increase or decrease in RRP for rift T1 is highly correlated ($r = 0.93$) with scatterometer derived MI variations. Meltwater is denser than ice. Thus meltwater percolating into the rift generates stress at the tip that could trigger rift propagation. In contrast to T1, poor correlation was observed between MI and RRP for rift T2 (Fig. 6c). This could be due to the

https://doi.org/10.1017/S0954102014000832 Published online by Cambridge University Press

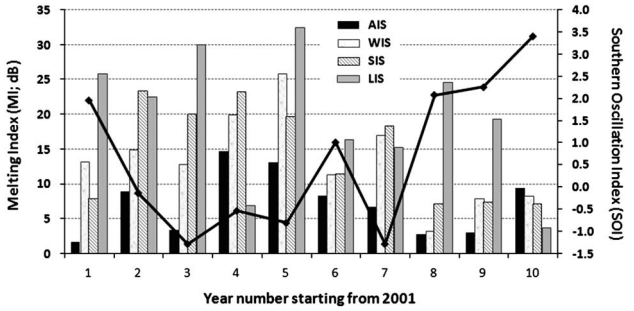


Fig. 7. Interannual variations of melting index (MI; dB) and Southern Oscillation Index (SOI). AIS = Amery, LIS = Larsen C, SIS = Shackleton, WIS = West ice shelves.

larger width of T2; surface melt driven mechanisms dominate on narrow rifts, but ocean swell and marine ice mechanisms may also play critical roles for a wide rift.

Southern Oscillation Index correlation with melting index

Figure 7 shows the yearly variations in average MI observed over LIS, AIS, SIS and WIS. Associated SOI values are also shown. Extreme melting events are generally coincident with strong negative SOI phase (SOI < -0.5). Strong positive SOI phase is associated with low surface melting, with some exceptions for LIS.

Regression analyses following Eqs (2), (3) & (4) show the dependence of MI on T_a and SOI (Table I). The r_1, r_2 and r_3 correlation coefficients are obtained from Eqs (2), (3) & (4), respectively. The value of a_1 is highest for LIS and lowest for AIS; indicating that the impact of change in T_a on surface melting is higher for LIS compared to AIS. Air temperature alone is insufficient to predict the change in MI for SIS; MI variations are better explained by SOI ($r_2 = 0.89$). Values of r_1 and r_2 obtained for WIS indicate the considerable influence of both parameters (T_a and SOI) on variations observed in MI. Incorporation of both parameters in Eq. (4) significantly improves the correlation coefficient (r_3) as seen in Table I. Findings suggest that ENSO signals represented by SOI explain some of the MI variance that remained unexplained after considering the effect of atmospheric temperature (T_a).

Table I. Summary of regression analysis for melting index–air temperature–Southern Oscillation Index relationships, following Eqs (2–4).

	Amery	West	Shackleton	Larsen C	All ice shelves†
a_1	2.17	3.17	2.49*	6.38	3.10
a_2	15.51	39.50	17.25	27.46	19.35
r_1	0.73	0.76	0.24	0.77	0.62
b_1	-1.79*	-3.20	-4.16	0.95*	-2.26
b_2	7.50	15.14	16.72	19.58	15.07
r_2	0.56	0.72	0.89	0.20	0.41
c_1	1.89	2.22	0.25*	7.21	3.09
c_2	-1.34*	-2.20	-4.12	3.15	-1.84
c_3	14.68	32.82	17.00	27.81	21.11
r_3	0.85	0.87	0.89	0.91	0.73

Melting index is measured in dB.
Results are statistically significant at 95% confidence level except for the cases indicated by *.
†The relationship developed by incorporating data points from all four ice shelves.

Discussion

Lower melting index pattern over large ice shelves

Very low intensity surface melting is observed (Fig. 1) over the large FRIS and RIS. Most mass loss from these ice shelves is by intermittent calving flux and basal melting (Hellmer *et al.* 2012, Depoorter *et al.* 2013, Rignot *et al.* 2013, Moholdt *et al.* 2014).

Melting index pattern over Larsen, Shackleton and West ice shelves

Over the study period, LIS showed high melting. This result is supported by the findings of Trusel *et al.* (2012), who reported >100 melt days per annum for LIS. In this region, mean summer temperatures have risen to near-melting and the length of the melt season has doubled over the past two decades (Glasser *et al.* 2009). This atmospheric warming could be a key factor for considerable surface melting evident over LIS. Such phenomena lead to acceleration of surface melt driven processes, such as meltwater ponds and downward penetration of water through crevasses. It has been suggested that meltwater acts as a mechanical force in crevasses, to cause fractures in the ice shelf leading to its disintegration (Scambos *et al.* 2003).

Similarly, high (> 60) numbers of melt days per annum support the decade long high MI values evident over SIS and WIS. The loss of ice mass from SIS and WIS is part of a long-term trend that has been evident since the early twentieth century (Young & Gibson 2007).

Impact of melting index on rift propagation

Episodic high melting events play a key role in the development of surface melt driven features, such as crevasses and rifts. Over the region of the AIS that covers the rift system (Figs 1, 2 & 5), the MI values were > 10 dB. Trusel *et al.* (2012) also reported this as the region of AIS most affected by melt.

Higher RRP during summer was reported by Fricker *et al.* (2005). Another important finding by Fricker *et al.* (2005) was an increasing RRP trend from 1996–2004, with an exception of a relative decrease in 2002–03. The relatively low RRP value reported in 2002–03 coincides with relatively low surface melting observed in the respective summer (Fig. 6b). However, for other years, with MI identical to 2003, lower rift propagation is observed (Fig. 6a). This indicates that other external forcings are also

https://doi.org/10.1017/S0954102014000832 Published online by Cambridge University Press

controlling rift propagation, e.g. ocean swells, tsunamis or interactions between crevasses and rifts (Walker *et al.* 2013).

Correlations with tropical Pacific Ocean variability

Oza *et al.* (2011) demonstrated that, as expected, monthly T_a in the summer (December and January) has an impact on the surface melting observed at various sites over AIS. As suggested by Scambos *et al.* (2003) for LIS, AIS may be susceptible to break up, subject to the continuation of a warming trend. In addition to T_a, as suggested by Turner (2004), variations in MI may be linked with the SOI. During the study period, strong melt summers (high MI) coincide with strongly negative SOI (Fig. 7). Tedesco & Monaghan (2009) also found similar anti-correlation between passive microwave radiometer based MI and SOI.

In the present study, 2.5° x 2.5° resolution NCEP/NCAR reanalysis of T_a data was utilized. The error in the NCEP/NCAR data could explain the lower correlation obtained for some ice shelves. Bromwich & Fogt (2004) indicate that ERA40 reanalysis perform better than NCEP/NCAR. However, as mentioned by Lampkin & Karmosky (2009), the quality of NCEP/NCAR output has been shown to be better for the summer, where more satellite information was fed into the reanalysis. In addition to the model error, T_a data could be contaminated by the contribution from the ice–ocean interface due to the coarse resolution grid. Further studies are planned to incorporate high spatial resolution satellite derived T_a, which enables pixel-level investigations.

Conclusions

The data available from Oceansat-2 OSCAT scatterometer extends the QuikSCAT scatterometer based time series of surface MI. Decadal (2000–10) spatial–temporal analysis of MI has been carried out over Antarctic ice shelves. Detailed investigations have been carried out for four ice shelves: LIS in West Antarctica and AIS, WIS and SIS in East Antarctica.

Low intensity surface melting was observed over the large ice shelves, FRIS and RIS. However, the high intensity surface melting observed for WIS and SIS is comparable with that observed for LIS. This confirms that ice shelves in East Antarctica are not immune from warming effects and demand constant monitoring.

The importance of scatterometer derived MI in understanding surface deformation changes have been demonstrated over AIS. Higher correlations were obtained between the MI and rift propagation for narrow rifts compared to wider rifts. The tropical linkage of MI with ENSO anomalies has been demonstrated. To conclude, ENSO and surface air temperature are important parameters influencing ice surface melting.

Acknowledgements

This work was carried out under projects funded by Space Applications Centre, Indian Space Research Organisation. The author is grateful to Dr R.R. Navalgund and Mr A.S. Kiran Kumar for their kind guidance provided to take up the polar science activities. Valuable suggestions received from Dr J.S. Parihar and Dr P.K. Pal are appreciatively acknowledged. Critical review and kind advice received from Dr Raj Kumar is deeply acknowledged. The author thankfully acknowledges the comments received from Dr M.P. Oza to improve the manuscript and to Mr D.A. Maroo for reproduction of figures in journal format. Thanks go to the comments and suggestions from two anonymous reviewers that prompted revisions that have led to a clearer presentation of the results of analysis and discussion. The valuable suggestions and encouragement during the revision process received from Dr L. Padman, journal Editor, are gratefully acknowledged. Efforts made by the editorial team to improve the manuscript are sincerely acknowledged.

Author contribution

Author confirms that the results and discussion provided in the article are based on his contribution. Entire manuscript has been prepared and all revisions were carried out only by the author.

References

Allison, I., Alley, R.B., Fricker, H.A., Thomas, R.H. & Warner, R.C. 2009. Ice sheet mass balance and sea level. *Antarctic Science*, **21**, 413–426.

Bassis, J.N., Fricker, H.A., Coleman, R., Bock, Y., Behrens, J., Darnell, D., Okal, M. & Minster, J.B. 2007. Seismicity and deformation associated with ice-shelf rift propagation. *Journal of Glaciology*, **53**, 523–536.

Bhowmick, S.A., Kumar, R. & Kumar, A.S.K. 2014. Cross calibration of the OceanSAT-2 scatterometer with QuikSCAT scatterometer using natural terrestrial targets. *IEEE Transactions on Geoscience and Remote Sensing*, **52**, 3393–3398.

Bromwich, D.H. & Fogt, R.L. 2004. Strong trends in the skill of the ERA-40 and NCEP-NCAR reanalysis in the high and mid latitudes of the Southern Hemisphere, 1958–2001. *Journal of Climate*, **17**, 4603–4619.

Depoorter, M.A., Bamber, J.L., Griggs, J.A., Lenaerts, J.T.M., Ligtenberg, S.R.M., van den Broeke, M.R. & Moholdt, G. 2013. Calving fluxes and basal melt rates of Antarctic ice shelves. *Nature*, **502**, 89–92.

Early, D.S. & Long, D.G. 2001. Image reconstruction and enhanced resolution imaging from irregular samples. *IEEE Transactions on Geoscience and Remote Sensing*, **39**, 291–302.

Fricker, H.A., Young, N.W., Coleman, R., Bassis, J.N. & Minster, J.B. 2005. Multi-year monitoring of rift propagation on the Amery Ice Shelf, East Antarctica. *Geophysical Research Letters*, **32**, 10.1029/2004GL021036.

Fung, A.K. 1994. *Microwave scattering and emission models and their applications*. Norwood: Artech House, 592 pp.

https://doi.org/10.1017/S0954102014000832 Published online by Cambridge University Press

Glasser, N.F., Kulessa, B., Luckman, A., Jansen, D., King, E.C., Sammonds, P.R., Scambos, T.A. & Jezek, K.C. 2009. Surface structure and stability of the Larsen C Ice Shelf, Antarctic Peninsula. *Journal of Glaciology*, **55**, 400–410.

Hellmer, H.H., Kauker, F., Timmermann, R., Determann, J. & Rae, J. 2012. Twenty-first-century warming of a large Antarctic ice-shelf cavity by a redirected coastal current. *Nature*, **485**, 225–228.

IPCC. 2013. *Climate change 2013: the physical science basis. Contribution of Working Group I to the Fifth Assessment Report of the Intergovernmental Panel on Climate Change*. New York, NY: Cambridge University Press, 3–29.

Lampkin, D.J. & Karmosky, C.C. 2009. Surface melt magnitude retrieval over Ross Ice Shelf, Antarctica using coupled MODIS near-IR and thermal satellite measurements. *The Cryosphere Discussion*, **3**, 1069–1107.

Liu, H., Wang, L. & Jezek, K.C. 2006. Spatiotemporal variations of snowmelt in Antarctica derived from satellite scanning multichannel microwave radiometer and Special Sensor Microwave Imager data (1978–2004). *Journal of Geophysical Research*, **111**, 10.1029/2005JF000318.

Long, D.G. & Drinkwater, M.R. 1994. Greenland observed at high resolution by the Seasat-A scatterometer. *Journal of Glaciology*, **32**, 213–230.

Munneke, P.K., Ligtenberg, S.R.M., van den Broeke, M.R. & Vaughan, D.G. 2014. Firn air depletion as precursor of Antarctic ice-shelf collapse. *Journal of Glaciology*, **60**, 205–214.

Moholdt, G., Padman, L. & Fricker, H.A. 2014. Basal mass budget of Ross and Filchner-Ronne ice shelves, Antarctica, derived from Lagrangian analysis of ICESat altimetry. *Journal of Geophysical Research - Earth Surface*, 10.1002/2014JF003171.

Oza, S.R., Singh, R.K.K, Vyas, N.K. & Sarkar, A. 2011. Study of inter-annual variations in surface melting over Amery Ice Shelf, East Antarctica using space-borne scatterometer data. *Journal of Earth System Science*, **120**, 329–336.

Picard, G. & Fily, M. 2006. Surface melting observations in Antarctica by microwave radiometers: correcting 26-year time series from changes in acquisition hours. *Remote Sensing of Environment*, **104**, 325–336.

Rignot, E., Jacobs, S., Mouginot, J. & Scheuchl, B. 2013. Ice shelf melting around Antarctica. *Science*, **341**, 266–270.

Scambos, T., Bohlander, J. & Raup, B. 1996. *Images of Antarctic ice shelves*. [December to February 2002–2010]. Boulder, CO: National Snow and Ice Data Center. Available at: http://nsidc.org/data/iceshelves_images/.

Scambos, T., Hulbe, C. & Fahnestock, M. 2003. Climate-induced ice shelf disintegration in the Antarctic Peninsula. *Antarctic Research Series*, **79**, 79–92.

Scambos, T., Ross, R., Bauer, R., Yermolin, Y., Skvarca, P., Long, D., Bohlander, J. & Haran, T. 2008. Calving and ice-shelf break-up processes investigated by proxy: Antarctic tabular iceberg evolution during northward drift. *Journal of Glaciology*, **54**, 579–591.

Tedesco, M. & Monaghan, A.J. 2009. An updated Antarctic melt record through 2009 and its linkages to high-latitude and tropical climate variability. *Geophysical Research Letters*, **36**, 10.1029/2009GL039186.

Trusel, L.D., Frey, K.E. & Das, S.B. 2012. Antarctic surface melting dynamics: enhanced perspectives from radar scatterometer data. *Journal of Geophysical Research - Earth Surface*, **117**, 10.1029/2011JF002126.

Turner, J. 2004. The El Nino–Southern Oscillation and Antarctica. *International Journal of Climatology*, **24**, 10.1002/joc.965.

Walker, C.C., Bassis, J.N., Fricker, H.A. & Czerwinski, R.J. 2013. Structural and environmental controls on Antarctic ice shelf rift propagation inferred from satellite monitoring. *Journal of Geophysical Research - Earth Surface*, **118**, 2354–2364.

Wismann, V. 2000. Monitoring of seasonal snowmelt on Greenland with ERS scatterometer data. *IEEE Transaction on Geoscience and Remote Sensing*, **38**, 1821–1826.

Young, N.W. & Gibson, J.A.E. 2007. A century of change in the Shackleton and West ice shelves, East Antarctica. *Geophysical Research Abstracts*, **9**, 10892.

https://doi.org/10.1017/S0954102014000832 Published online by Cambridge University Press